

# Robust 3D Shape Reconstruction in Zero-Shot from a Single Image in the Wild

Junhyeong Cho<sup>1</sup> Kim Youwang<sup>2</sup> Hunmin Yang<sup>1,3</sup> Tae-Hyun Oh<sup>2,4</sup>

<sup>1</sup>ADD <sup>2</sup>Department of Electrical Engineering, POSTECH

<sup>3</sup>Department of Mechanical Engineering, KAIST <sup>4</sup>School of Computing, KAIST

<https://ZeroShape-W.github.io>

## Abstract

Recent monocular 3D shape reconstruction methods have shown promising zero-shot results on object-segmented images without any occlusions. However, their effectiveness is significantly compromised in real-world conditions, due to imperfect object segmentation by off-the-shelf models and the prevalence of occlusions. To effectively address these issues, we propose **a unified regression model** that integrates segmentation and reconstruction, specifically designed for occlusion-aware 3D shape reconstruction. To facilitate its reconstruction in the wild, we also introduce **a scalable data synthesis pipeline** that simulates a wide range of variations in objects, occluders, and backgrounds. Training on our synthetic data enables the proposed model to achieve state-of-the-art zero-shot results on real-world images, using significantly fewer parameters than competing approaches.

## 1. Introduction

The abundance of large-scale 3D shapes [5, 8, 12, 20, 40] has enabled the development of reconstruction models with strong generalization capabilities, even allowing for zero-shot monocular 3D shape reconstruction [31, 35, 49, 77, 79, 85]. However, these models are not deployable in real-world settings, as they assume object images that have no backgrounds and occlusions. Thus, they utilize *off-the-shelf* segmentation models [39, 69] to handle in-the-wild images. This dependency introduces two main challenges: (i) error accumulation by off-the-shelf models, and (ii) removal of occluded object parts by segmentation. Both issues hinder precise shape reconstruction, as shown in Figure 1.

To tackle the challenges, we propose **ZeroShape-W**, an occlusion-aware 3D shape reconstruction model (Fig. 2a). Our model jointly regresses the silhouettes of a salient object and its occluders, along with a depth map and camera intrinsics to estimate the object’s visible 3D shape. Then, its full 3D shape is reconstructed by using the visible 3D shape and the silhouette of occluders. This approach enables the reconstruction of occluded object parts, making it effective



Figure 1. Single-view 3D shape reconstruction on real-world images [76]. Compared with LRM [31] that requires an off-the-shelf segmentation model (e.g., SAM [39]), our approach not only eliminates the need for such an additional model but also achieves greater robustness to occlusions.

in real-world conditions. However, a significant challenge remains: *how can we train our model for robust zero-shot reconstruction in the wild?* To achieve this goal, we need large-scale diverse data that can cover various real environments. Unfortunately, the availability of real-world images annotated with precise 3D shapes is limited. An alternative approach is to generate realistic renderings from 3D object collections [5, 8, 12, 13, 20], but this is also limited by the availability of high-quality synthetic assets.

In this paper, we introduce a scalable data synthesis pipeline (Fig. 2b) that simulates a wide range of variations using generative models, thereby removing the reliance on limited real-world data or high-quality synthetic assets. Our pipeline first synthesizes foreground object images using a conditional generative model [97], with spatial conditions obtained by rendering 3D shapes available from extensive object collections [5, 12, 13]. Then, their backgrounds are generated by an object-aware background outpainting model [16]. For these synthesized images, we apply Copy-Paste augmentation [25] to simulate occluders on-the-fly during model training.

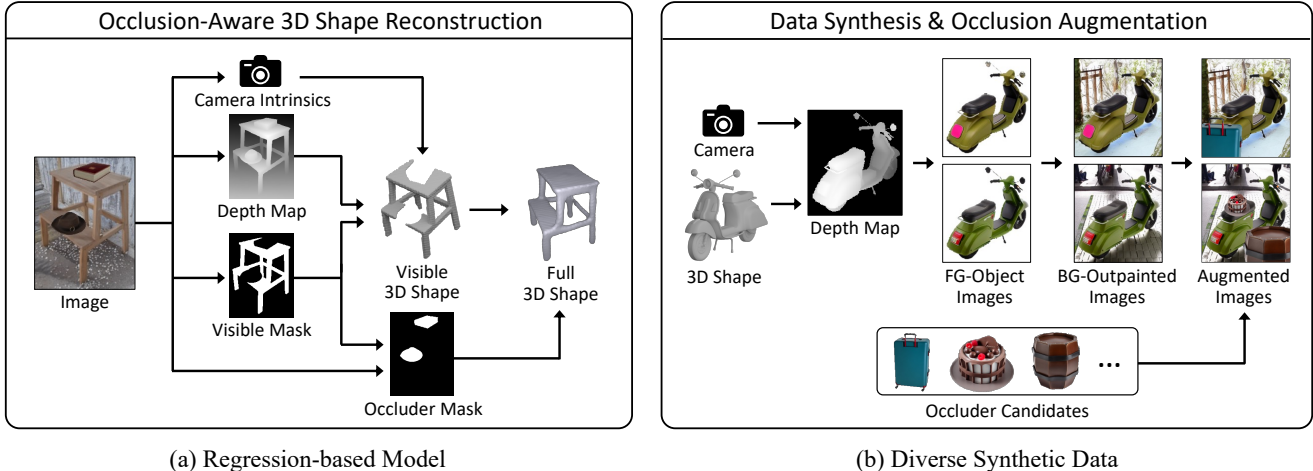


Figure 2. Proposed approach for zero-shot monocular 3D shape reconstruction in the wild. (a) Our model reconstructs the full 3D shape of a salient object using its visible 3D shape and the silhouette of its occluders. The visible 3D shape is estimated from camera intrinsics, depth map, and visible region of the object. (b) We create our training dataset by synthesizing diverse data. We render 3D shapes and then simulate their appearances and backgrounds using generative models. Occluders are inserted on-the-fly during model training.

By training the proposed model on our diverse synthetic data, we expose it to a wide variety of foreground objects, their occluders, and backgrounds. This process enables our model to focus on learning to capture domain-invariant and object-centric geometric priors. In this way, we improve its generalization across various environments.

To validate the effectiveness of our approach, we first create our training dataset by synthesizing diverse images using 3D shapes from Objaverse [13] and ShapeNet [5]. Then, we train our model on the data augmented with occlusions. We evaluate the model on the real-world benchmark, Pix3D [76], where it outperforms state-of-the-art models while using significantly fewer model parameters. In addition to the benchmark, we also qualitatively evaluate the proposed model on in-the-wild images from ObjectNet [2], OfficeHome [83], and PACS [42].

## 2. Related Work

**Single-view 3D shape reconstruction in the wild.** This task aims to estimate the 3D shape of an object from a single image captured in a real-world environment. It is challenging because objects exhibit a variety of 3D shapes while their appearances are greatly altered by environmental factors. To handle such variations, 3D shape reconstruction models [1, 7, 24, 26–29, 31, 34–36, 46, 49, 56, 59, 62, 77, 79, 81, 84, 85, 87–89, 91, 92, 94, 96, 99] should generalize well across various environments. However, the scarcity of real-world 3D data poses a significant obstacle in pursuing this goal. In this paper, we address this issue by synthesizing large-scale data using generative models.

Single-view reconstruction methods fall into two categories: generative model-based approaches [49, 77, 85, 92] and regression-based approaches [31, 35, 79]. The genera-

tive model-based approaches synthesize multi-view images using diffusion models such as Zero-1-to-3 [47], which are effective to estimate 3D shapes with textures but incur significant computational costs. In contrast, regression-based approaches such as ZeroShape [35] estimate 3D shapes in a single forward pass, offering much greater efficiency.

Recent state-of-the-art methods in both approaches assume clean object-segmented images without occlusions, making them difficult to operate in real-world settings. In this work, we tackle this issue by introducing a unified regression model that both segments and reconstructs while accounting for occlusions. To the best of our knowledge, our work is the first regression-based approach for zero-shot single-view 3D shape reconstruction in the wild.

**Improving model robustness to distribution shifts.** It is common to exploit multiple domains for learning domain-invariant features [4, 15, 37, 41, 43, 52, 53, 73, 101, 102] to enhance the model robustness. However, multiple domains from real-world environments might not be accessible. To effectively tackle this issue, domain randomization methods [11, 18, 32, 54, 65, 70, 78, 80, 95] synthesize multiple domains via a random simulation of diverse scenarios. By exposing a model to randomized variations, it learns to capture generalizable representations capable of handling a wide range of variations encountered in real-world settings.

Following the paradigm of domain randomization, we simulate diverse variations in foreground objects, occluders, and backgrounds. However, this is not done completely randomly, as the background outpainting model [16] generates backgrounds while considering the foreground objects. By training the proposed model on our data, it could learn to capture domain-invariant and object-centric geometric priors, which are useful for handling diverse objects.

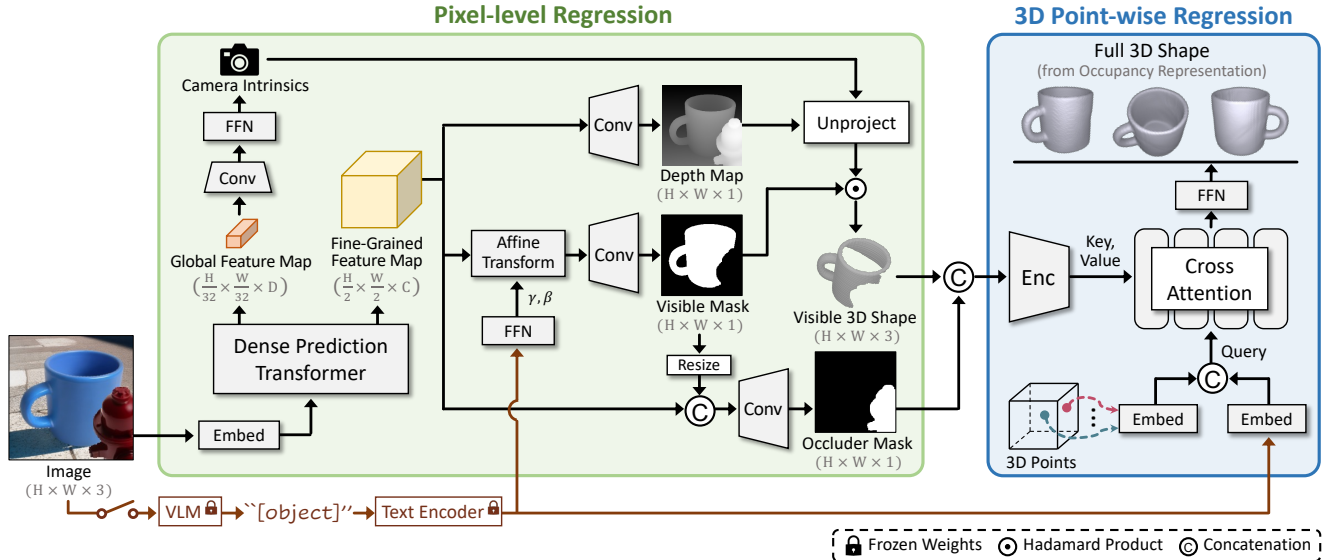


Figure 3. Overall architecture of ZeroShape-W. Given an object-centric RGB image, our model leverages the backbone of Dense Prediction Transformer (DPT) [68] to regress camera intrinsics, a depth map, a visible mask of a salient object, and an occluder mask that represents the object’s occluders. These components are used to derive the object’s visible 3D shape, which is then combined with the occluder mask to regress occupancy values of 3D point queries through cross-attention layers [82]. This process recovers the object’s full 3D shape, including occluded object parts. To alleviate difficulties of in-the-wild reconstruction, we optionally incorporate open-set category priors by estimating the object’s category, “[object]” (e.g., “cup”), using an additional vision-language model (VLM) [45].

**Synthetic data generation.** To train 3D shape reconstruction models, we can synthesize data by rendering 3D objects from extensive object collections [5, 8, 12, 13, 20, 40] via computer graphics tools. As long as sufficient 3D shape and texture assets are available for objects and environments, this approach could also facilitate 3D shape reconstruction in the wild. However, it is expensive to collect a great variety of high-quality assets (e.g., 4K-resolution texture maps, HDR environment maps) needed to bridge the gap between synthetic and real environments. Moreover, the diversity of object appearances and backgrounds depicted by rendered images is determined by the combination of available assets. Compared with these computer graphics tools, our data synthesis pipeline could simulate more diverse object appearances and backgrounds without relying on such additional high-quality assets, by leveraging generative models pre-trained on large-scale datasets.

**Generative models with 3D assets.** Recent works [23, 51, 98] use conditional generative models [57, 66, 97] to synthesize images with 3D assets for various tasks, e.g., object pose estimation. Compared with them, accurate preservation of silhouettes within spatial conditions is more crucial for 3D shape reconstruction. To better preserve silhouettes, our data synthesis pipeline employs a two-step generation process. We utilize an initial guidance for foreground object synthesis and exploit a background outpainting model [16] specifically designed for preserving silhouettes. In this way, each synthesized image is paired with its precise 3D shape.



Figure 4. Effect of using an occluder mask. It enables full 3D shape reconstruction, even for occluded object parts. Note that existing state-of-the-art methods [31, 35, 49, 77, 79, 85] struggle with occlusions, as they assume the salient visible object in the current view is unobstructed.

### 3. Method

The proposed ZeroShape-W (Fig. 3) aims to regress the full 3D shape of a salient object from a single image, including its visible and occluded parts (Fig. 4). Inspired by [35, 86], our model first regresses pixel-level information, which is used as condition to regress occupancy values of 3D point queries. These occupancy values represent the visible and hidden geometry of the salient object, while also accounting for occluded regions that were not addressed in [35, 86].

During pixel-level regression, our model regresses a depth map, a visible mask of the object, and an occluder mask that depicts the object’s occluders. It also estimates camera intrinsics to convert depth values into the object’s visible 3D shape in a viewer-centric coordinate system.

During 3D point-wise regression, our model regresses occupancy values of 3D point queries through cross-attention layers [82], utilizing features from the visible 3D shape and occluder mask as keys and values. This approach

can effectively reconstruct the object’s hidden geometry, with the help of learned 3D shape priors.

For in-the-wild images, identifying arbitrary salient objects is often challenging due to complex backgrounds or occlusions, which can result in noisy mask estimations. In such cases, visible 3D shapes may mistakenly include background geometries. To address these issues, we optionally incorporate category-specific priors by leveraging a vision-language model [45] and CLIP text encoder [67]. Specifically, the vision-language model generates a **category-specific prompt** “[object]” (e.g., “cup” in Fig. 3) that describes the salient object in the input image. For stable inference with unseen object categories, we use an averaged CLIP text embedding obtained from the category-specific prompt and a **category-agnostic prompt** “object”. In cases where the category-specific priors are not used, our model relies solely on the category-agnostic prompt without estimating the object’s category.

### 3.1. Pixel-level Regression

For an object-centric RGB image  $I \in \mathbb{R}^{H \times W \times 3}$ , we first obtain image embeddings  $\mathbf{E}_I \in \mathbb{R}^{(H/16) \times (W/16) \times D}$  using ResNet50 [30], as done in ViT-Hybrid [14]. Then, we feed the embeddings  $\mathbf{E}_I$  into the backbone of Dense Prediction Transformer (DPT) [68]. From the backbone, we extract a global feature map  $\mathbf{X}_G \in \mathbb{R}^{(H/32) \times (W/32) \times D}$  and a fine-grained feature map  $\mathbf{X}_F \in \mathbb{R}^{(H/2) \times (W/2) \times C}$ . The global feature map  $\mathbf{X}_G$  is the reassembled output from the last transformer layer in DPT, while the fine-grained feature map  $\mathbf{X}_F$  is the output from the last fusion layer in DPT.

**Camera intrinsics.** To regress the visible 3D shape of the salient object, we estimate camera intrinsics  $K \in \mathbb{R}^{3 \times 3}$  from the global feature map  $\mathbf{X}_G$ . Specifically, we obtain the camera intrinsics  $K$  by predicting a focal length scaling factor and principal point shifts, as done in [35]. The scaling factor adjusts a base focal length according to the image resolution  $H \times W$ , and the principal point shifts are also specified relative to the image resolution. These parameters are estimated from the global feature map  $\mathbf{X}_G$  using shallow convolutional layers, a pooling layer, and a feed forward network (FFN).

**Depth map.** To derive the visible 3D shape by unprojecting depth values using the estimated camera intrinsics  $K$ , we regress a depth map  $\mathbf{M}_D \in \mathbb{R}^{H \times W \times 1}$  from the fine-grained feature map  $\mathbf{X}_F$ . For this regression, we use shallow convolutional layers with interpolation.

**Visible mask.** To identify the visible region of the salient object, we regress a visible mask  $\mathbf{M}_V \in \mathbb{R}^{H \times W \times 1}$  from the fine-grained feature map  $\mathbf{X}_F$ . For precise regression, we adaptively adjust the fine-grained feature map  $\mathbf{X}_F$  based on the object’s category. Inspired by [31, 63, 64], we modulate the feature map using an affine transformation with a scaling factor  $\gamma \in \mathbb{R}^C$  and a shift factor  $\beta \in \mathbb{R}^C$ , estimated

by an FFN with CLIP text encoder [67]. We modulate the feature map  $\mathbf{X}_F$  at each spatial location  $(i, j)$  as follows:

$$\bar{\mathbf{X}}_{F_{ij}} = (1 + \gamma)\mathbf{X}_{F_{ij}} + \beta, \quad (1)$$

where  $\bar{\mathbf{X}}_F \in \mathbb{R}^{(H/2) \times (W/2) \times C}$ . From this modulated feature map, we regress the visible mask  $\mathbf{M}_V$  using shallow convolutional layers with interpolation.

**Visible 3D shape.** Using the estimated camera intrinsics  $K$ , depth map  $\mathbf{M}_D$ , and visible mask  $\mathbf{M}_V$ , we derive the visible 3D shape  $\mathbf{S}_V \in \mathbb{R}^{H \times W \times 3}$  that contains  $(x, y, z)$ -coordinates of each pixel location  $(i, j)$  as follows:

$$\mathbf{S}_{V_{ij}} = \mathbb{1}_{\{\mathbf{M}_{V_{ij}} \geq \eta\}} \cdot (\mathbf{M}_{D_{ij}} K^{-1} [i, j, 1]^\top), \quad (2)$$

where  $\mathbb{1}_{\{\cdot\}}$  is an indicator function, and  $\eta$  denotes a threshold. We normalize  $\mathbf{S}_V$  to have a zero mean and a unit scale.

**Occluder mask.** To determine the object’s occluded region, we regress an occluder mask  $\mathbf{M}_O \in \mathbb{R}^{H \times W \times 1}$  using the fine-grained feature map  $\mathbf{X}_F$  and visible mask  $\mathbf{M}_V$ . Specifically, we resize the visible mask to the resolution of  $H/2 \times W/2$ , and concatenate it with the feature map along the channel dimension. Then, we regress the occluder mask  $\mathbf{M}_O$  using shallow convolutional layers with interpolation.

### 3.2. 3D Point-wise Regression

We regress occupancy values of 3D point queries using cross-attention layers to effectively consider local features from pixel-level estimations.<sup>1</sup> We begin by concatenating the visible 3D shape  $\mathbf{S}_V$  and the occluder mask  $\mathbf{M}_O$  along the channel dimension, which is then fed into an encoder. It produces  $Z$ -dimensional vectors that serve as keys and values in cross-attention layers.

For each 3D point query, we construct a  $Z$ -dimensional query vector by concatenating two  $Z/2$ -dimensional embeddings: one from the point’s  $(x, y, z)$ -coordinates and the other from CLIP text encoder [67]. The query vectors are processed through  $L$  cross-attention layers, where each query independently attends to its relevant spatial features. Then, to reconstruct the object’s full 3D shape, we estimate the occupancy value of each query using an FFN.

### 3.3. Loss

We train our model using binary cross-entropy losses with the estimated visible mask  $\mathbf{M}_V$ , occluder mask  $\mathbf{M}_O$ , and occupancy values. For the estimated depth map  $\mathbf{M}_D$ , we apply a scale- and shift-invariant MAE loss [19] over two regions: (i) the visible mask region with ground-truth depth and (ii) the entire region with pseudo depth estimated from a pre-trained model, referred to as the auxiliary depth loss. This auxiliary loss addresses the limitation of our data synthesis pipeline, which only provides depth for object areas. For the estimated camera intrinsics  $K$ , we use an MSE loss by comparing the visible 3D shape  $\mathbf{S}_V$  to the ground truth.

<sup>1</sup>We extend prior works [35, 86] to reconstruct occluded object parts.

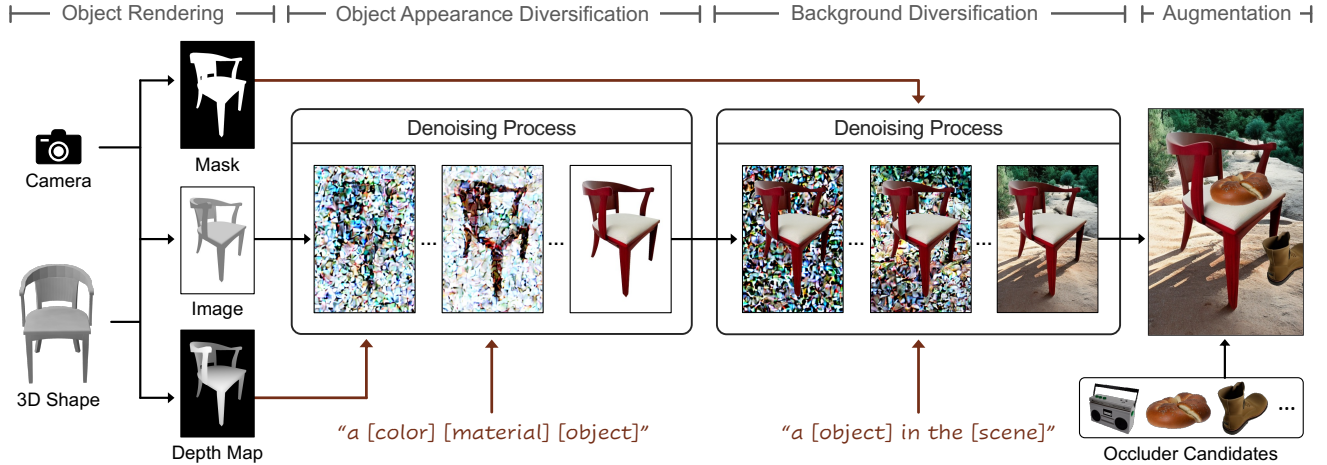


Figure 5. Overview of our data synthesis. Given a camera and 3D object, we render it to obtain an object mask, image, and depth map. We simulate object appearances via a conditional diffusion model [97] using the depth as its spatial condition and “a [color] [material] [object]” (e.g., “a red wood chair”) as its textual condition. To alleviate shape distortion by the generative model, we use the rendered image as initial guidance. We simulate its background via an object-aware background outpainting model [16] using the mask and “a [object] in the [scene]” (e.g., “a chair in the canyon”) as its textual condition. Then, we put occluders during data augmentation.

### 3.4. Implementation Details

We input an image of resolution  $H \times W$ , where  $H = W = 224$ . Using DPT-Hybrid [68], we extract the  $D$ -dimensional feature  $\mathbf{X}_G$  and  $C$ -dimensional feature  $\mathbf{X}_F$ , where  $D = 768$  and  $C = 256$ . In eq. (2), we set  $\eta = 0.5$ . In  $L$  cross-attention layers, we employ  $Z$ -dimensional vectors, where  $L = 2$  and  $Z = 256$ . During training, we use Depth Anything V2 [93] for the auxiliary depth loss. At inference time, we optionally use LLaMA-VID [45] to identify the object’s category. Further details can be found in the supplementary material.

## 4. Data Synthesis

Our scalable data synthesis pipeline (Fig. 5) produces diverse images, along with their corresponding 3D shapes, camera parameters, depth maps, and masks. We use Copy-Paste [25] augmentation to insert occluders at each training iteration. Please see the supplementary material for details.

### 4.1. Object Rendering

A great variety of 3D shapes can be readily obtained from 3D object collections [5, 8, 12, 13, 20, 40] or generative models [6, 48, 74, 88]. In line with ZeroShape [35], we utilize the same set of 3D objects spanning over 1,000 categories, including 52K objects from ShapeNetCore.v2 [5] and 42K objects from Objaverse-LVIS [13].

Each 3D object is rendered by multiple cameras constructed with varying camera distances, elevation angles, focal lengths, and LookAt points. This rendering process produces over 1 million object images, and each output is paired with precise 3D shapes, camera parameters, depth maps, and masks.

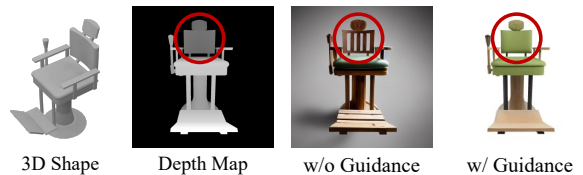


Figure 6. Effect of using an initial guidance. The guidance assists in preserving the object silhouette depicted in the spatial condition.

### 4.2. Object Appearance Diversification

To simulate diverse visual variations in object appearances, we employ ControlNet [97] which is a conditional diffusion model capable of realistically synthesizing diverse images. In our data synthesis, the generative model simulates a wide range of variations by using a depth map as its spatial condition and “a [color] [material] [object]” as its textual condition. Here, the placeholders [color] and [material] are replaced by words selected from predefined color and material lists, while [object] denotes the category of the used 3D object.

**Initial guidance.** The diffusion model [97] occasionally distorts the object silhouette depicted in the spatial condition. To alleviate this distortion, we utilize the rendered image as initial guidance. Motivated by SDEdit [55], we perturb the guidance with Gaussian noise and feed it to the model. Since the noisy guidance retains the original spatial structure, it effectively reduces silhouette distortion (Fig. 6).

### 4.3. Background Diversification

To simulate diverse backgrounds, we use an object-aware background outpainting model [16]. It adapts Stable Diffusion Inpainting 2.0 [71] by using modified ControlNet [97], allowing for background generation without extending the

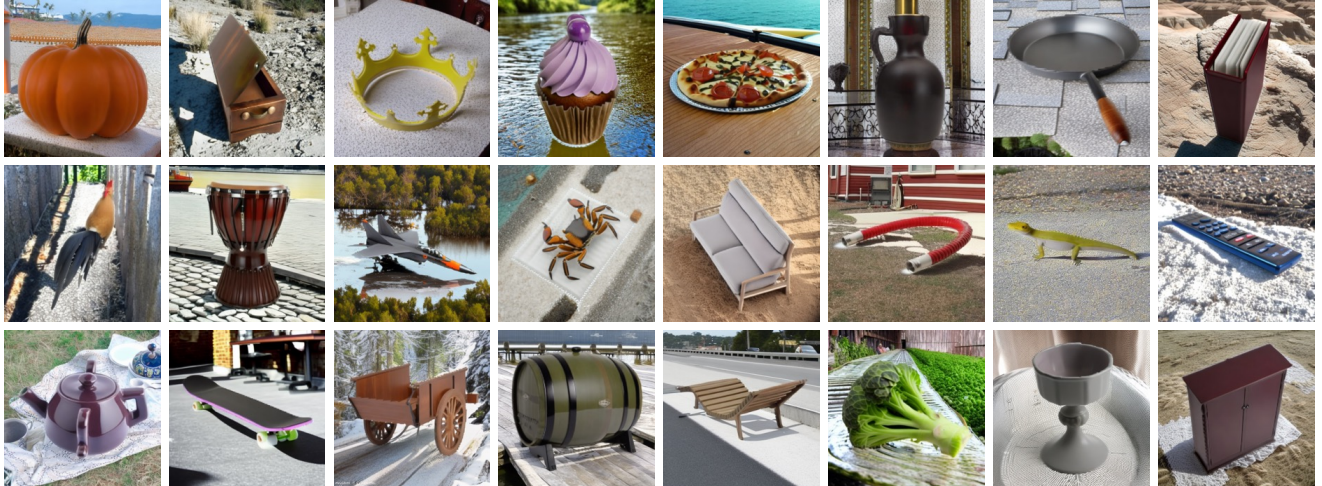


Figure 7. Diverse synthetic data produced by our scalable data synthesis pipeline. Based on 3D shape renderings from ShapeNetCore.v2 [5] and Objaverse-LVIS [13], we synthesize diverse images using ControlNet [97] and object-aware background outpainting model [16].

object’s silhouette. We generate various backgrounds using the object image, its mask, and the prompt “a [object] in the [scene]”, where [scene] is selected from scene categories [90, 100]. Ideally, it synthesizes backgrounds that appear to be captured by cameras with focal lengths similar to those used for the object’s rendering.

#### 4.4. Augmentation

For images generated by our data synthesis (Fig. 7), we simulate occluders on-the-fly during model training via Copy-Paste augmentation [25] using our synthesized foreground objects. To enable stable estimation of camera intrinsics, we put objects rendered by similar focal lengths.

### 5. Experiments

#### 5.1. Evaluation Settings

**Protocol.** To convert implicit 3D shape representation into explicit 3D meshes, we extract the isosurface from the implicit representation via the Marching Cubes [50] algorithm. Following [29, 59, 96], we align predicted and ground-truth meshes using the Iterative Closest Point algorithm. Then, we uniformly sample 10K points from each mesh.

**Metrics.** Using 10K sampled points, we compute Chamfer Distance (CD) and F-Score (FS) for quantitative evaluation, as in [33–35]. Specifically,  $FS@_\tau$  denotes the harmonic mean of  $precision@_\tau$  and  $recall@_\tau$ , which represents the concordance between predicted and ground-truth points within a distance threshold  $\tau$ .

**Datasets.** We evaluate our model on real-world object images from Pix3D [76], ObjectNet [2], OfficeHome [83], and PACS [42]. As Pix3D is the widely recognized benchmark for 3D shape reconstruction in the wild, we use it for comparison with other state-of-the-art models [31, 35].

#### 5.2. Experimental Results

**Quantitative comparison.** Currently, there is no zero-shot monocular 3D shape reconstruction model capable of directly processing in-the-wild images. Therefore, we compare our model with state-of-the-art reconstruction models, LRM [31]<sup>2</sup> and ZeroShape [35], which operate on object-segmented images without occlusions. For comprehensive comparisons with these baselines, we equip them with the off-the-shelf modal segmentation model, SAM [39], and amodal completion model, pix2gestalt [61].

In Table 1, we evaluate the baselines and our model on the Pix3D benchmark [76]. Although the proposed model does not utilize such off-the-shelf models, it substantially outperforms them. In terms of  $FS@_\tau$ , our model outperforms the strongest baseline  $ZeroShape_w/SAM + pix2gestalt$  by a large margin of 13.7% (38.2 vs. 33.6). With regard to CD, the proposed model also surpasses the strongest baseline by a large margin of 13.4% (0.097 vs. 0.110); lower is better for CD evaluation metric.

Our model requires significantly fewer parameters than the baselines, since it performs joint regression using the shared feature map  $X_F$ . For example, the number of parameters used by our model is less than 1/12 of the parameters used by  $LRM_w/SAM + pix2gestalt$ , as shown in Table 1.

**Qualitative comparison.** Figure 8 presents single-view 3D shape reconstruction results on real-world images from Pix3D [76]. When existing reconstruction models [31, 35] utilize an off-the-shelf modal segmentation model [39], they struggle to estimate the geometry for occluded object parts. To enable occlusion-aware 3D reconstruction, they should incorporate an amodal completion model [61]. However,

<sup>2</sup>In this paper, we use the publicly available OpenLRM model weights from <https://github.com/3DTopia/OpenLRM>

Model	Off-the-shelf Model		Overhead #Params	Pix3D Evaluation				
	Modal Segmentation	Amodal Completion		FS@ $\tau$ ↑	FS@ $2\tau$ ↑	FS@ $3\tau$ ↑	FS@ $5\tau$ ↑	CD↓
LRM	SAM	—	> 1100M	31.0	54.5	69.9	87.1	0.121
	SAM	pix2gestalt	> 2400M	31.1	54.9	70.6	87.7	0.119
ZeroShape	SAM	—	> 800M	32.1	56.8	72.1	88.0	0.116
	SAM	pix2gestalt	> 2100M	33.6	59.0	74.2	89.2	0.110
<b>Ours (category-agnostic)</b>	—	—	<b>193.7M</b>	<b>38.2</b>	<b>65.3</b>	<b>79.9</b>	<b>92.5</b>	<b>0.097</b>

Table 1. Comparison of single-view 3D shape reconstruction on Pix3D [76]. Existing state-of-the-art reconstruction models, LRM [31] and ZeroShape [35], require an off-the-shelf modal segmentation model (e.g., SAM [39]), because they assume object-segmented images without any occlusions. For occlusion-aware reconstruction, they need an additional amodal completion model (e.g., pix2gestalt [61]). In this comparison, our model is evaluated using the category-agnostic prompt “object”.

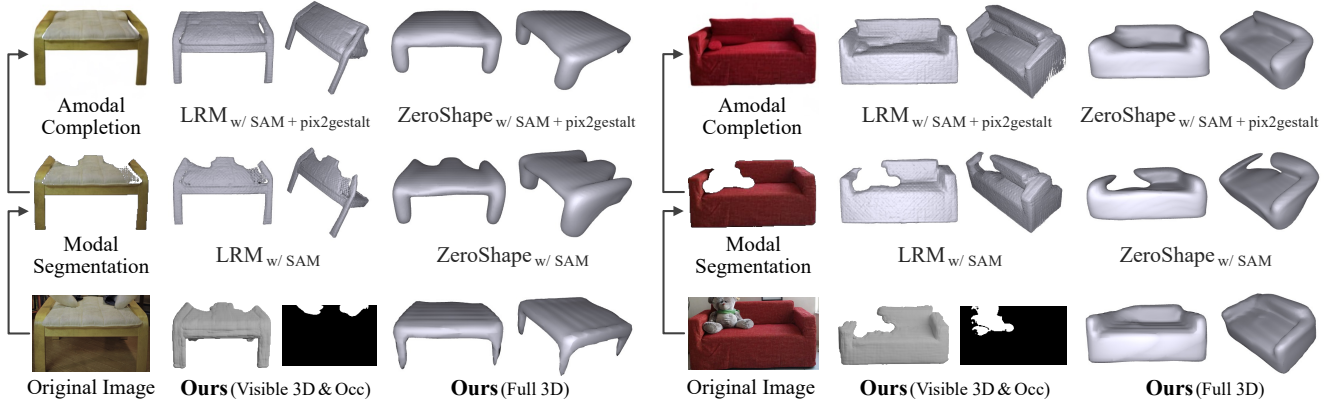


Figure 8. Comparison of single-view 3D shape reconstruction on Pix3D [76]. In this comparison, LRM [31] and ZeroShape [35] take modal segmentation results (from SAM [39]) or amodal completion results (from pix2gestalt [61]) as inputs. In contrast, our model directly takes original images as inputs, and performs occlusion-aware reconstruction by regressing visible 3D shapes and occluder silhouettes.

this approach often leads to error accumulation. Even with well-completed amodal images, shape reconstruction errors may still occur (see LRM<sub>w/SAM</sub>+pix2gestalt in the left column of Figure 8). This might be due to compatibility issues with off-the-shelf models, as they were trained on different datasets. In contrast, our model achieves promising results without the need to heavily pre-process input images using the off-the-shelf models.

**Evaluation on non-occluded or occluded images only.** In Table 2, we compare evaluation results on non-occluded or occluded object images from the Pix3D dataset [76], which consists of 42.6% non-occluded and 57.4% occluded images. Under both scenarios, our end-to-end regression method substantially outperforms existing approaches [31, 35] that depend on an off-the-shelf model [39].

**Optional category-specific priors.** To evaluate the effect of incorporating such category priors, we compare results obtained using the category-agnostic prompt “object” and the category-specific prompt “[object]” (estimated by a VLM [45]). Table 3 shows that the priors improve our model’s accuracy. Please see the supplementary material for more analyses.

Model	Non-Occluded		Occluded	
	FS@ $\tau$ ↑	CD↓	FS@ $\tau$ ↑	CD↓
LRM <sub>w/SAM</sub>	33.5	0.111	29.1	0.128
ZeroShape <sub>w/SAM</sub>	34.6	0.106	30.2	0.123
<b>Ours (category-agnostic)</b>	<b>43.6</b>	<b>0.082</b>	<b>34.2</b>	<b>0.107</b>

Table 2. Quantitative evaluation exclusively on *non-occluded* or *occluded* object images from the Pix3D dataset [76].

Prompt	Pix3D Evaluation		
	FS@ $\tau$ ↑	FS@ $5\tau$ ↑	CD↓
Category Agnostic	38.2	92.5	0.097
Category Specific (w/ VLM)	<b>39.1</b>	<b>92.6</b>	<b>0.095</b>

Table 3. Pix3D [76] evaluation according to category prompts. We incorporate category-specific priors by using a VLM [45].

**Reconstruction of diverse objects.** Figure 9 presents single-view 3D shape reconstruction results on real-world images from ObjectNet [2], OfficeHome [83], and PACS [42]. By leveraging learned priors, the proposed model can regress 3D shapes of various objects captured in real-world environments.



Figure 9. Single-view 3D shape reconstruction of diverse object shapes. We qualitatively evaluate our model on real-world object images from ObjectNet [2], OfficeHome [83], and PACS [42]. The proposed model achieves promising in-the-wild reconstruction results, which demonstrates that our regression-based model has effectively learned generalizable 3D shape priors.

Model	Pix3D Evaluation		
	FS@ $\tau$ $\uparrow$	FS@5 $\tau$ $\uparrow$	CD $\downarrow$
<i>w/o auxiliary depth*</i>	35.9	90.7	0.105
<i>w/o occluders*</i>	37.7	91.2	0.102
<i>w/o text prompt</i>	38.0	91.5	0.101
<b>Ours (category-specific)*</b>	<b>39.6</b>	<b>92.8</b>	<b>0.094</b>

Table 4. Effects of key components. On Pix3D [76], we analyze the accuracy of our model by ablating each component. \* denotes using ground-truth object names for category-specific prompts.

### 5.3. Ablation Study

**Effect of auxiliary depth loss.** In the absence of this loss, we observe that predicted depth values for non-object regions are not precise, leading to worse results (see *w/o auxiliary depth* in Table 4). This depth loss helps to accurately regress depth values across the entire image, which aids in distinguishing the salient object from its occluders and backgrounds based on depth. Moreover, the auxiliary loss prevents our model from overfitting to the training data.

**Effect of simulating occluders.** Without the Copy-Paste augmentation and the occluder mask estimation branch, our model struggles to reconstruct the full 3D shape when the salient object is occluded. Although this variant estimates visible 3D shapes fairly well in the absence of occlusions, its overall accuracy is degraded on in-the-wild images from the Pix3D dataset [76] (see *w/o occluders* in Table 4).

**Effect of text prompt.** When we do not use text prompts, our model sometimes incorrectly splits a single object into visible and occluder regions based on depth. In addition, it struggles to handle noisy visible 3D shapes that contain background geometries by mistake. As a result, its accuracy is diminished (see *w/o text prompt* in Table 4).

Model	Train GPUs	Feat. Res.	Train Res.	Inference Res.
LRM	128 A100	32×32	128×128×128	384×384×384
Ours	4 RTX3090	14×14	32×32×32	128×128×128

Table 5. Used resources and resolutions. *Feat. Res.* denotes image feature resolutions from DINOv2 [60] or ResNet50 [30], while *Train/Inference Res.* indicate spatial resolutions.

## 6. Limitations

**Lack of training resources.** As shown in Table 5, resolutions differ significantly due to limited resources (*i.e.*, 4 RTX3090 vs. 128 A100). Consequently, our reconstructed 3D shapes appear smoother than the shapes from LRM [31].

**Challenges with boundary-clipped objects.** Our model can handle occlusions, but it may struggle to estimate the geometry of object parts clipped by image boundaries.

**Dataset ambiguity.** Ambiguity in the dataset may hinder our model’s ability to distinguish the salient object from its occluders. For example, some “bed” 3D objects only consist of bed frames, while others include pillows.

**Unrealistic occluders.** Copy-Paste augmentations have proven effective [25], but they introduce a domain gap when compared to actual occluders in real-world environments.

## 7. Conclusion

To enable zero-shot single-view reconstruction in the wild, we presented (i) a unified regression model for occlusion-aware 3D shape reconstruction, and (ii) a scalable data synthesis pipeline for creating training dataset. Our approach achieved state-of-the-art accuracy on in-the-wild images. Unlike other existing methods, our method does not utilize off-the-shelf segmentation or amodal completion models, leading to significantly fewer model parameters.

**Acknowledgments.** This work was supported by ADD grant funded by the Korean government. T.-H. Oh and K. Youwang were partially supported by Institute of Information & communications Technology Planning & Evaluation (IITP) grant (No. RS-2024-00457882, National AI Research Lab Project; No. RS-2020-II200004, Development of Previsional Intelligence based on Long-term Visual Memory Network), and National Research Foundation of Korea (NRF) grant (No. RS-2024-00358135, Corner Vision: Learning to Look Around the Corner through Multimodal Signals) funded by the Korean government (MSIT).

## References

- [1] Kalyan Vasudev Alwala, Abhinav Gupta, and Shubham Tulsiani. Pre-train, Self-train, Distill: A simple recipe for Supersizing 3D Reconstruction. In *Proceedings of the IEEE/CVF Conference on Computer Vision and Pattern Recognition (CVPR)*, 2022. 2
- [2] Andrei Barbu, David Mayo, Julian Alverio, William Luo, Christopher Wang, Dan Gutfreund, Josh Tenenbaum, and Boris Katz. Objectnet: A large-scale bias-controlled dataset for pushing the limits of object recognition models. In *Advances in Neural Information Processing Systems (NeurIPS)*, 2019. 2, 6, 7, 8
- [3] Nicholas Carlini, Florian Tramèr, Eric Wallace, Matthew Jagielski, Ariel Herbert-Voss, Katherine Lee, Adam Roberts, Tom Brown, Dawn Song, Ulfar Erlingsson, Alina Oprea, and Colin Raffel. Extracting Training Data from Large Language Models. In *30th USENIX Security Symposium (USENIX Security 21)*, 2021. 17
- [4] Fabio Maria Carlucci, Antonio D’Innocente, Silvia Bucci, Barbara Caputo, and Tatiana Tommasi. Domain Generalization by Solving Jigsaw Puzzles. In *Proceedings of the IEEE/CVF Conference on Computer Vision and Pattern Recognition (CVPR)*, 2019. 2
- [5] Angel X. Chang, Thomas Funkhouser, Leonidas Guibas, Pat Hanrahan, Qixing Huang, Zimo Li, Silvio Savarese, Manolis Savva, Shuran Song, Hao Su, Jianxiong Xiao, Li Yi, and Fisher Yu. ShapeNet: An Information-Rich 3D Model Repository. *arXiv preprint arXiv:1512.03012*, 2015. 1, 2, 3, 5, 6, 16
- [6] Gene Chou, Yuval Bahat, and Felix Heide. Diffusion-SDF: Conditional Generative Modeling of Signed Distance Functions. In *Proceedings of the IEEE/CVF International Conference on Computer Vision (ICCV)*, 2023. 5
- [7] Christopher B. Choy, Danfei Xu, JunYoung Gwak, Kevin Chen, and Silvio Savarese. 3D-R2N2: A Unified Approach for Single and Multi-view 3D Object Reconstruction. In *Proceedings of the European Conference on Computer Vision (ECCV)*, 2016. 2
- [8] Jasmine Collins, Shubham Goel, Kenan Deng, Achleshwar Luthra, Leon Xu, Erhan Gundogdu, Xi Zhang, Tomas F. Yago Vicente, Thomas Dideriksen, Himanshu Arora, Matthieu Guillaumin, and Jitendra Malik. ABO: Dataset and Benchmarks for Real-World 3D Object Understanding. In *Proceedings of the IEEE/CVF Conference on Computer Vision and Pattern Recognition (CVPR)*, 2022. 1, 3, 5
- [9] Blender Online Community. Blender - a 3D modelling and rendering package. *Blender Foundation*, 2018. 14
- [10] Terrance de Vries, Ishan Misra, Changhan Wang, and Laurens van der Maaten. Does Object Recognition Work for Everyone? In *Proceedings of the IEEE/CVF Conference on Computer Vision and Pattern Recognition (CVPR) Workshops*, 2019. 17
- [11] Atabak Dehban, João Borrego, Rui Figueiredo, Plinio Moreno, Alexandre Bernardino, and Josá Santos-Victor. The impact of domain randomization on object detection: A case study on parametric shapes and synthetic textures. In *IEEE/RSJ International Conference on Intelligent Robots and Systems (IROS)*, 2019. 2
- [12] Matt Deitke, Ruoshi Liu, Matthew Wallingford, Huong Ngo, Oscar Michel, Aditya Kusupati, Alan Fan, Christian Laforte, Vikram Voleti, Samir Yitzhak Gadre, Eli VanderBilt, Aniruddha Kembhavi, Carl Vondrick, Georgia Gkioxari, Kiana Ehsani, Ludwig Schmidt, and Ali Farhadi. Objaverse-XL: A Universe of 10M+ 3D Objects. In *Advances in Neural Information Processing Systems (NeurIPS)*, 2023. 1, 3, 5
- [13] Matt Deitke, Dustin Schwenk, Jordi Salvador, Luca Weihs, Oscar Michel, Eli VanderBilt, Ludwig Schmidt, Kiana Ehsani, Aniruddha Kembhavi, and Ali Farhadi. Objaverse: A Universe of Annotated 3D Objects. In *Proceedings of the IEEE/CVF Conference on Computer Vision and Pattern Recognition (CVPR)*, 2023. 1, 2, 3, 5, 6, 14, 16
- [14] Alexey Dosovitskiy, Lucas Beyer, Alexander Kolesnikov, Dirk Weissenborn, Xiaohua Zhai, Thomas Unterthiner, Mostafa Dehghani, Matthias Minderer, Georg Heigold, Sylvain Gelly, Jakob Uszkoreit, and Neil Houlsby. An Image is Worth 16x16 Words: Transformers for Image Recognition at Scale. In *International Conference on Learning Representations (ICLR)*, 2021. 4
- [15] Qi Dou, Daniel C. Castro, Konstantinos Kamnitsas, and Ben Glocker. Domain Generalization via Model-Agnostic Learning of Semantic Features. In *Advances in Neural Information Processing Systems (NeurIPS)*, 2019. 2
- [16] Amir Erfan Eshratifar, Joao V. B. Soares, Kapil Thadani, Shaunak Mishra, Mikhail Kuznetsov, Yueh-Ning Ku, and Paloma de Juan. Salient Object-Aware Background Generation using Text-Guided Diffusion Models. In *Proceedings of the IEEE/CVF Conference on Computer Vision and Pattern Recognition (CVPR) Workshops*, 2024. 1, 2, 3, 5, 6, 14, 17
- [17] Patrick Esser, Robin Rombach, and Björn Ommer. A Note on Data Biases in Generative Models. In *NeurIPS 2020 Workshop on Machine Learning for Creativity and Design*, 2020. 17
- [18] Ioannis Exarchos, Yifeng Jiang, Wenhao Yu, and C. Karen Liu. Policy Transfer via Kinematic Domain Randomization and Adaptation. In *International Conference on Robotics and Automation (ICRA)*, 2021. 2
- [19] Towards Robust Monocular Depth Estimation: Mixing Datasets for Zero-shot Cross-dataset Transfer. René

- Ranftl and Katrin Lasinger and David Hafner and Konrad Schindler and Vladlen Koltun. *IEEE Transactions on Pattern Analysis and Machine Intelligence (TPAMI)*, 2020. 4
- [20] Huan Fu, Rongfei Jia, Lin Gao, Mingming Gong, Binqiang Zhao, Steve Maybank, and Dacheng Tao. 3D-FUTURE: 3D Furniture shape with TextURE. In *International Journal of Computer Vision (IJCV)*, 2021. 1, 3, 5
- [21] Rohit Gandikota, Joanna Materzynska, Jaden Fiotto-Kaufman, and David Bau. Erasing Concepts from Diffusion Models. In *Proceedings of the IEEE/CVF International Conference on Computer Vision (ICCV)*, 2023. 17
- [22] Jakob Gawlikowski, Cedricque Rovile Njicutcheu Tassi, Mohsin Ali, Jongseok Lee, Matthias Humt, Jianxiang Feng, Anna Kruspe, Rudolph Triebel, Peter Jung, Ribana Roscher, Muhammad Shahzad, Wen Yang, Richard Bamler, and Xiao Xiang Zhu. A survey of uncertainty in deep neural networks. *Artificial Intelligence Review*, 2023. 17
- [23] Yongtao Ge, Wenjia Wang, Yongfan Chen, Hao Chen, and Chunhua Shen. 3D Human Reconstruction in the Wild with Synthetic Data Using Generative Models. *arXiv preprint arXiv:2403.11111*, 2024. 3
- [24] Kyle Genova, Forrester Cole, Avneesh Sud, Aaron Sarna, and Thomas Funkhouser. Local Deep Implicit Functions for 3D Shape. In *Proceedings of the IEEE/CVF Conference on Computer Vision and Pattern Recognition (CVPR)*, 2020. 2
- [25] Golnaz Ghiasi, Yin Cui, Aravind Srinivas, Rui Qian, Tsung-Yi Lin, Ekin D. Cubuk, Quoc V. Le, and Barret Zoph. Simple Copy-Paste is a Strong Data Augmentation Method for Instance Segmentation. In *Proceedings of the IEEE/CVF Conference on Computer Vision and Pattern Recognition (CVPR)*, 2021. 1, 5, 6, 8
- [26] Rohit Girdhar, David F. Fouhey, Mikel Rodriguez, and Abhinav Gupta. Learning a Predictable and Generative Vector Representation for Objects. In *Proceedings of the European Conference on Computer Vision (ECCV)*, 2016. 2
- [27] Georgia Gkioxari, Jitendra Malik, and Justin Johnson. Mesh R-CNN. In *Proceedings of the IEEE/CVF International Conference on Computer Vision (ICCV)*, 2019.
- [28] Shubham Goel, Angjoo Kanazawa, and Jitendra Malik. Shape and Viewpoint without Keypoints. In *Proceedings of the European Conference on Computer Vision (ECCV)*, 2020.
- [29] Thibault Groueix, Matthew Fisher, Vladimir G. Kim, Bryan C. Russell, and Mathieu Aubry. AtlasNet: A Papier-Mâché Approach to Learning 3D Surface Generation. In *Proceedings of the IEEE Conference on Computer Vision and Pattern Recognition (CVPR)*, 2018. 2, 6
- [30] He, Kaiming and Zhang, Xiangyu and Ren, Shaoqing and Sun, Jian. Deep Residual Learning for Image Recognition. In *Proceedings of the IEEE Conference on Computer Vision and Pattern Recognition (CVPR)*, pages 770–778, 2016. 4, 8, 14
- [31] Yicong Hong, Kai Zhang, Jiuxiang Gu, Sai Bi, Yang Zhou, Difan Liu, Feng Liu, Kalyan Sunkavalli, Trung Bui, and Hao Tan. LRM: Large Reconstruction Model for Single Image to 3D. In *International Conference on Learning Representations (ICLR)*, 2024. 1, 2, 3, 4, 6, 7, 8
- [32] Jiaxing Huang, Dayan Guan, Aoran Xiao, and Shijian Lu. FSDR: Frequency Space Domain Randomization for Domain Generalization. In *Proceedings of the IEEE/CVF Conference on Computer Vision and Pattern Recognition (CVPR)*, 2021. 2
- [33] Zixuan Huang, Stefan Stojanov, Anh Thai, Varun Jampani, and James M. Rehg. Planes vs. Chairs: Category-guided 3D shape learning without any 3D cues. In *Proceedings of the European Conference on Computer Vision (ECCV)*, 2022. 6
- [34] Zixuan Huang, Varun Jampani, Anh Thai, Yuanzhen Li, Stefan Stojanov, and James M. Rehg. ShapeClipper: Scalable 3D Shape Learning from Single-View Images via Geometric and CLIP-based Consistency. In *Proceedings of the IEEE/CVF Conference on Computer Vision and Pattern Recognition (CVPR)*, 2023. 2
- [35] Zixuan Huang, Stefan Stojanov, Anh Thai, Varun Jampani, and James M. Rehg. ZeroShape: Regression-based Zero-shot Shape Reconstruction. In *Proceedings of the IEEE/CVF Conference on Computer Vision and Pattern Recognition (CVPR)*, 2024. 1, 2, 3, 4, 5, 6, 7, 14, 15
- [36] Angjoo Kanazawa, Shubham Tulsiani, Alexei A. Efros, and Jitendra Malik. Learning Category-Specific Mesh Reconstruction from Image Collections. In *Proceedings of the European Conference on Computer Vision (ECCV)*, 2018. 2
- [37] Donghyun Kim, Kuniaki Saito, Tae-Hyun Oh, Bryan A. Plummer, Stan Sclaroff, and Kate Saenko. Cross-domain Self-supervised Learning for Domain Adaptation with Few Source Labels. In *Proceedings of the IEEE/CVF International Conference on Computer Vision (ICCV)*, 2021. 2
- [38] Diederik P. Kingma and Jimmy Ba. Adam: A Method for Stochastic Optimization. In *International Conference on Learning Representations (ICLR)*, 2015. 15
- [39] Alexander Kirillov, Eric Mintun, Nikhila Ravi, Hanzi Mao, Chloe Rolland, Laura Gustafson, Tete Xiao, Spencer Whitehead, Alexander C. Berg, Wan-Yen Lo, Piotr Dollár, and Ross Girshick. Segment Anything. In *Proceedings of the IEEE/CVF International Conference on Computer Vision (ICCV)*, 2023. 1, 6, 7
- [40] Sebastian Koch, Albert Matveev, Zhongshi Jiang, Francis Williams, Alexey Artemov, Evgeny Burnaev, Marc Alexa, Denis Zorin, and Daniele Panozzo. ABC: A Big CAD Model Dataset For Geometric Deep Learning. In *Proceedings of the IEEE/CVF Conference on Computer Vision and Pattern Recognition (CVPR)*, 2019. 1, 3, 5
- [41] Pang Wei Koh, Shiori Sagawa, Henrik Marklund, Sang Michael Xie, Marvin Zhang, Akshay Balsubramani, Weihua Hu, Michihiro Yasunaga, Richard Lanus Phillips, Irena Gao, Tony Lee, Etienne David, Ian Stavness, Wei Guo, Berton A. Earnshaw, Imran S. Haque, Sara Beery, Jure Leskovec, Anshul Kundaje, Emma Pierson, Sergey Levine, Chelsea Finn, and Percy Liang. WILDS: A Benchmark of in-the-Wild Distribution Shifts. In *International Conference on Machine Learning (ICML)*, 2021. 2
- [42] Da Li, Yongxin Yang, Yi-Zhe Song, and Timothy M. Hospedales. Deeper, Broader and Artier Domain Gener-

- alization. In *Proceedings of the IEEE International Conference on Computer Vision (ICCV)*, 2017. 2, 6, 7, 8
- [43] Da Li, Jianshu Zhang, Yongxin Yang, Cong Liu, Yi-Zhe Song, and Timothy M. Hospedales. Episodic Training for Domain Generalization. In *Proceedings of the IEEE/CVF International Conference on Computer Vision (ICCV)*, 2019. 2
- [44] Yuheng Li, Haotian Liu, Qingyang Wu, Fangzhou Mu, Jianwei Yang, Jianfeng Gao, Chunyuan Li, and Yong Jae Lee. GLIGEN: Open-Set Grounded Text-to-Image Generation. In *Proceedings of the IEEE/CVF Conference on Computer Vision and Pattern Recognition (CVPR)*, 2023. 17
- [45] Yanwei Li, Chengyao Wang, and Jiaya Jia. LLaMA-VID: An Image is Worth 2 Tokens in Large Language Models. In *Proceedings of the European Conference on Computer Vision (ECCV)*, 2024. 3, 4, 5, 7, 14, 15, 16
- [46] Haolin Liu, Yujian Zheng, Guanying Chen, Shuguang Cui, and Xiaoguang Han. Towards High-Fidelity Single-view Holistic Reconstruction of Indoor Scenes. In *Proceedings of the European Conference on Computer Vision (ECCV)*, 2022. 2
- [47] Ruoshi Liu, Rundi Wu, Basile Van Hoorick, Pavel Tokmakov, Sergey Zakharov, and Carl Vondrick. Zero-1-to-3: Zero-shot One Image to 3D Object. In *Proceedings of the IEEE/CVF International Conference on Computer Vision (ICCV)*, 2023. 2
- [48] Zhen Liu, Yao Feng, Michael J. Black, Derek Nowrouzezahrai, Liam Paull, and Weiyang Liu. MeshDiffusion: Score-based Generative 3D Mesh Modeling. In *International Conference on Learning Representations (ICLR)*, 2023. 5
- [49] Xiaoxiao Long, Yuan-Chen Guo, Cheng Lin, Yuan Liu, Zhiyang Dou, Lingjie Liu, Yuexin Ma, Song-Hai Zhang, Marc Habermann, Christian Theobalt, and Wenping Wang. Wonder3D: Single Image to 3D using Cross-Domain Diffusion. In *Proceedings of the IEEE/CVF Conference on Computer Vision and Pattern Recognition (CVPR)*, 2024. 1, 2, 3
- [50] William E. Lorensen and Harvey E. Cline. Marching cubes: A high resolution 3D surface construction algorithm. *ACM SIGGRAPH Computer Graphics*, 21(4), 1987. 6, 16
- [51] Wufei Ma, Qihao Liu, Jiahao Wang, Angtian Wang, Xiaoding Yuan, Yi Zhang, Zihao Xiao, Guofeng Zhang, Beijia Lu, Ruxiao Duan, Yongrui Qi, Adam Kortylewski, Yaoyao Liu, and Alan Yuille. Generating Images with 3D Annotations Using Diffusion Models. In *International Conference on Learning Representations (ICLR)*, 2024. 3
- [52] Divyat Mahajan, Shruti Tople, and Amit Sharma. Domain Generalization using Causal Matching. In *International Conference on Machine Learning (ICML)*, 2021. 2
- [53] Toshihiko Matsuura and Tatsuya Harada. Domain Generalization Using a Mixture of Multiple Latent Domains. In *Proceedings of the AAAI Conference on Artificial Intelligence (AAAI)*, 2020. 2
- [54] Bhairav Mehta, Manfred Diaz, Florian Golemo, Christopher J. Pal, and Liam Paull. Active Domain Randomization. In *Conference on Robot Learning (CoRL)*, 2019. 2
- [55] Chenlin Meng, Yutong He, Yang Song, Jiaming Song, Jianjun Wu, Jun-Yan Zhu, and Stefano Ermon. SDEdit: Guided Image Synthesis and Editing with Stochastic Differential Equations. In *International Conference on Learning Representations (ICLR)*, 2022. 5
- [56] Lars Mescheder, Michael Oechsle, Michael Niemeyer, Sebastian Nowozin, and Andreas Geiger. Occupancy Networks: Learning 3D Reconstruction in Function Space. In *Proceedings of the IEEE/CVF Conference on Computer Vision and Pattern Recognition (CVPR)*, 2019. 2
- [57] Chong Mou, Xintao Wang, Liangbin Xie, Yanze Wu, Jian Zhang, Zhongang Qi, Ying Shan, and Xiaohu Qie. T2I-Adapter: Learning Adapters to Dig out More Controllable Ability for Text-to-Image Diffusion Models. *arXiv preprint arXiv:2302.08453*, 2023. 3, 17
- [58] Zixuan Ni, Longhui Wei, Jiacheng Li, Siliang Tang, Yueting Zhuang, and Qi Tian. Degeneration-Tuning: Using Scrambled Grid shield Unwanted Concepts from Stable Diffusion. In *31st ACM International Conference on Multimedia*, 2023. 17
- [59] Yinyu Nie, Xiaoguang Han, Shihui Guo, Yujian Zheng, Jian Chang, and Jian Jun Zhang. Total3DUnderstanding: Joint Layout, Object Pose and Mesh Reconstruction for Indoor Scenes from a Single Image. In *Proceedings of the IEEE/CVF Conference on Computer Vision and Pattern Recognition (CVPR)*, 2020. 2, 6
- [60] Maxime Oquab, Timothée Darcet, Théo Moutakanni, Huy Vo, Marc Szafraniec, Vasil Khalidov, Pierre Fernandez, Daniel Haziza, Francisco Massa, Alaaeldin El-Nouby, Mahmoud Assran, Nicolas Ballas, Wojciech Galuba, Russell Howes, Po-Yao Huang, Shang-Wen Li, Ishan Misra, Michael Rabbat, Vasu Sharma, Gabriel Synnaeve, Hu Xu, Hervé Jegou, Julien Mairal, Patrick Labatut, Armand Joulin, and Piotr Bojanowski. DINOv2: Learning Robust Visual Features without Supervision. In *Transactions on Machine Learning Research*, 2024. 8
- [61] Ege Ozguroglu, Ruoshi Liu, Dídac Surís, Dian Chen, Achal Dave, Pavel Tokmakov, and Carl Vondrick. pix2gestalt: Amodal Segmentation by Synthesizing Wholes. In *Proceedings of the IEEE/CVF Conference on Computer Vision and Pattern Recognition (CVPR)*, 2024. 6, 7
- [62] Junyi Pan, Xiaoguang Han, Weikai Chen, Jiapeng Tang, and Kui Jia. Deep Mesh Reconstruction from Single RGB Images via Topology Modification Networks. In *Proceedings of the IEEE/CVF International Conference on Computer Vision (ICCV)*, 2019. 2
- [63] William Peebles and Saining Xie. Scalable Diffusion Models with Transformers. In *Proceedings of the IEEE/CVF International Conference on Computer Vision (ICCV)*, 2023. 4
- [64] Ethan Perez, Florian Strub, Harm de Vries, Vincent Dumoulin, and Aaron Courville. FiLM: Visual Reasoning with a General Conditioning Layer. In *Proceedings of the AAAI Conference on Artificial Intelligence (AAAI)*, 2018. 4
- [65] Aayush Prakash, Shaad Boochoon, Mark Brophy, David Acuna, Eric Cameracci, Gavriel State, Omer Shapira, and Stan Birchfield. Structured Domain Randomization: Bridging the Reality Gap by Context-Aware Synthetic Data.

- In *International Conference on Robotics and Automation (ICRA)*, 2019. 2
- [66] Can Qin, Shu Zhang, Ning Yu, Yihao Feng, Xinyi Yang, Yingbo Zhou, Huan Wang, Juan Carlos Niebles, Caiming Xiong, Silvio Savarese, Stefano Ermon, Yun Fu, and Ran Xu. UniControl: A Unified Diffusion Model for Controllable Visual Generation In the Wild. In *Advances in Neural Information Processing Systems (NeurIPS)*, 2023. 3, 17
- [67] Alec Radford, Jong Wook Kim, Chris Hallacy, Aditya Ramesh, Gabriel Goh, Sandhini Agarwal, Girish Sastry, Amanda Askell, Pamela Mishkin, Jack Clark, Gretchen Krueger, and Ilya Sutskever. Learning Transferable Visual Models From Natural Language Supervision. In *International Conference on Machine Learning (ICML)*, 2021. 4, 14, 16
- [68] René Ranftl, Alexey Bochkovskiy, and Vladlen Koltun. Vision Transformers for Dense Prediction. In *Proceedings of the IEEE/CVF International Conference on Computer Vision (ICCV)*, 2021. 3, 4, 5, 14, 15
- [69] Nikhila Ravi, Valentin Gabeur, Yuan-Ting Hu, Ronghang Hu, Chaitanya Ryali, Tengyu Ma, Haitham Khedr, Roman Rädle, Chloe Rolland, Laura Gustafson, Eric Mintun, Junting Pan, Kalyan Vasudev Alwala, Nicolas Carion, Chao-Yuan Wu, Ross Girshick, Piotr Dollár, and Christoph Feichtenhofer. SAM 2: Segment Anything in Images and Videos. *arXiv preprint arXiv:2408.00714*, 2024. 1
- [70] Xinyi Ren, Jianlan Luo, Eugen Solowjow, Juan Aparicio Ojea, Abhishek Gupta, Aviv Tamar, and Pieter Abbeel. Domain Randomization for Active Pose Estimation. In *International Conference on Robotics and Automation (ICRA)*, 2019. 2
- [71] Robin Rombach, Andreas Blattmann, Dominik Lorenz, Patrick Esser, and Björn Ommer. High-Resolution Image Synthesis with Latent Diffusion Models. In *Proceedings of the IEEE/CVF Conference on Computer Vision and Pattern Recognition (CVPR)*, 2022. 5
- [72] Akash Sengupta, Ignas Budvytis, and Roberto Cipolla. Humaniflow: Ancestor-conditioned normalising flows on so(3) manifolds for human pose and shape distribution estimation. In *Proceedings of the IEEE/CVF Conference on Computer Vision and Pattern Recognition (CVPR)*, 2023. 17
- [73] Seonguk Seo, Yumin Suh, Dongwan Kim, Geeho Kim, Jongwoo Han, and Bohyung Han. Learning to Optimize Domain Specific Normalization for Domain Generalization. In *Proceedings of the European Conference on Computer Vision (ECCV)*, 2020. 2
- [74] Jaehyeok Shim, Changwoo Kang, and Kyungdon Joo. Diffusion-Based Signed Distance Fields for 3D Shape Generation. In *Proceedings of the IEEE/CVF Conference on Computer Vision and Pattern Recognition (CVPR)*, 2023. 5
- [75] Jiaming Song, Chenlin Meng, and Stefano Ermon. Denoising Diffusion Implicit Models. In *International Conference on Learning Representations (ICLR)*, 2021. 14
- [76] Xingyuan Sun, Jiajun Wu, Xiuming Zhang, Zhoutong Zhang, Chengkai Zhang, Tianfan Xue, Joshua B. Tenenbaum, and William T. Freeman. Pix3D: Dataset and Methods for Single-Image 3D Shape Modeling. In *Proceedings of the IEEE/CVF Conference on Computer Vision and Pattern Recognition (CVPR)*, 2018. 1, 2, 6, 7, 8
- [77] Jiayang Tang, Zhaoxi Chen, Xiaokang Chen, Tengfei Wang, Gang Zeng, and Ziwei Liu. LGM: Large Multi-View Gaussian Model for High-Resolution 3D Content Creation. In *Proceedings of the European Conference on Computer Vision (ECCV)*, 2024. 1, 2, 3
- [78] Josh Tobin, Rachel Fong, Alex Ray, Jonas Schneider, Wojciech Zaremba, and Pieter Abbeel. Domain Randomization for Transferring Deep Neural Networks from Simulation to the Real World. In *IEEE/RSJ International Conference on Intelligent Robots and Systems (IROS)*, 2017. 2
- [79] Dmitry Tochilkin, David Pankratz, Zexiang Liu, Zixuan Huang, Adam Letts, Yangguang Li, Ding Liang, Christian Laforte, Varun Jampani, and Yan-Pei Cao. TripoSR: Fast 3D Object Reconstruction from a Single Image. *arXiv preprint arXiv:2403.02151*, 2024. 1, 2, 3
- [80] Jonathan Tremblay, Aayush Prakash, David Acuna, Mark Brophy, Varun Jampani, Cem Anil, Thang To, Eric Cameracci, Shaad Boochoon, and Stan Birchfield. Training Deep Networks With Synthetic Data: Bridging the Reality Gap by Domain Randomization. In *IEEE Conference on Computer Vision and Pattern Recognition (CVPR) Workshops*, 2018. 2
- [81] Shubham Tulsiani, Tinghui Zhou, Alexei A Efros, and Jitendra Malik. Multi-view supervision for single-view reconstruction via differentiable ray consistency. In *Proceedings of the IEEE Conference on Computer Vision and Pattern Recognition (CVPR)*, 2017. 2
- [82] Ashish Vaswani, Noam Shazeer, Niki Parmar, Jakob Uszkoreit, Llion Jones, Aidan N Gomez, Łukasz Kaiser, and Illia Polosukhin. Attention is All you Need. In *Advances in Neural Information Processing Systems (NIPS)*, 2017. 3
- [83] Hemanth Venkateswara, Jose Eusebio, Shayok Chakraborty, and Sethuraman Panchanathan. Deep Hashing Network for Unsupervised Domain Adaptation. In *Proceedings of the IEEE Conference on Computer Vision and Pattern Recognition (CVPR)*, 2017. 2, 6, 7, 8
- [84] Nanyang Wang, Yinda Zhang, Zhuwen Li, Yanwei Fu, Wei Liu, and Yu-Gang Jiang. Pixel2Mesh: Generating 3D Mesh Models from Single RGB Images. In *Proceedings of the European Conference on Computer Vision (ECCV)*, 2018. 2
- [85] Zhengyi Wang, Yikai Wang, Yifei Chen, Chendong Xiang, Shuo Chen, Dajiang Yu, Chongxuan Li, Hang Su, and Jun Zhu. CRM: Single Image to 3D Textured Mesh with Convolutional Reconstruction Model. In *Proceedings of the European Conference on Computer Vision (ECCV)*, 2024. 1, 2, 3
- [86] Chao-Yuan Wu, Justin Johnson, Jitendra Malik, Christoph Feichtenhofer, and Georgia Gkioxari. Multiview Compressive Coding for 3D Reconstruction. In *Proceedings of the IEEE/CVF Conference on Computer Vision and Pattern Recognition (CVPR)*, 2023. 3, 4
- [87] Jiajun Wu, Yifan Wang, Tianfan Xue, Xingyuan Sun, William T Freeman, and Joshua B Tenenbaum. MarrNet:

- 3D Shape Reconstruction via 2.5D Sketches. In *Advances in Neural Information Processing Systems (NIPS)*, 2017. 2
- [88] Jiajun Wu, Chengkai Zhang, Tianfan Xue, William T. Freeman, and Joshua B. Tenenbaum. Learning a Probabilistic Latent Space of Object Shapes via 3D Generative-Adversarial Modeling. In *Advances in Neural Information Processing Systems (NIPS)*, 2017. 5
- [89] Jiajun Wu, Chengkai Zhang, Xiuming Zhang, Zhoutong Zhang, William T. Freeman, and Joshua B. Tenenbaum. Learning Shape Priors for Single-View 3D Completion and Reconstruction. In *Proceedings of the European Conference on Computer Vision (ECCV)*, 2018. 2
- [90] Jianxiong Xiao, James Hays, Krista A. Ehinger, Aude Oliva, and Antonio Torralba. SUN database: Large-scale scene recognition from abbey to zoo. In *Proceedings of the IEEE Conference on Computer Vision and Pattern Recognition (CVPR)*, 2010. 6, 14
- [91] Yiheng Xiong and Angela Dai. Pt43d: A probabilistic transformer for generating 3d shapes from single highly-ambiguous rgb images. In *Proceedings of the British Machine Vision Conference (BMVC)*, 2024. 2, 17
- [92] Jiale Xu, Weihao Cheng, Yiming Gao, Xintao Wang, Shenghua Gao, and Ying Shan. InstantMesh: Efficient 3D Mesh Generation from a Single Image with Sparse-view Large Reconstruction Models. *arXiv preprint arXiv:2404.07191*, 2024. 2
- [93] Lihe Yang, Bingyi Kang, Zilong Huang, Zhen Zhao, Xiaogang Xu, Jiashi Feng, and Hengshuang Zhao. Depth Anything V2. In *Advances in Neural Information Processing Systems (NeurIPS)*, 2024. 5, 15
- [94] Kim Yu-Ji, Hyunwoo Ha, Kim Youwang, Jaeheung Surh, Hyowon Ha, and Tae-Hyun Oh. Metta: Single-view to 3d textured mesh reconstruction with test-time adaptation. In *Proceedings of the British Machine Vision Conference (BMVC)*, 2024. 2
- [95] Xiangyu Yue, Yang Zhang, Sicheng Zhao, Alberto Sangiovanni-Vincentelli, Kurt Keutzer, and Boqing Gong. Domain Randomization and Pyramid Consistency: Simulation-to-Real Generalization Without Accessing Target Domain Data. In *Proceedings of the IEEE/CVF International Conference on Computer Vision (ICCV)*, 2019. 2
- [96] Cheng Zhang, Zhaopeng Cui, Yinda Zhang, Bing Zeng, Marc Pollefeys, and Shuaicheng Liu. Holistic 3D Scene Understanding from a Single Image with Implicit Representation. In *Proceedings of the IEEE/CVF Conference on Computer Vision and Pattern Recognition (CVPR)*, 2021. 2, 6
- [97] Lvmin Zhang, Anyi Rao, and Maneesh Agrawala. Adding Conditional Control to Text-to-Image Diffusion Models. In *Proceedings of the IEEE/CVF International Conference on Computer Vision (ICCV)*, 2023. 1, 3, 5, 6, 14, 17
- [98] Mengqi Zhang, Yang Fu, Zheng Ding, Sifei Liu, Zhuowen Tu, and Xiaolong Wang. HOIDiffusion: Generating Realistic 3D Hand-Object Interaction Data. In *Proceedings of the IEEE/CVF Conference on Computer Vision and Pattern Recognition (CVPR)*, 2024. 3
- [99] Xiuming Zhang, Zhoutong Zhang, Chengkai Zhang, Joshua B. Tenenbaum, William T. Freeman, and Jiajun Wu. Learning to Reconstruct Shapes from Unseen Classes. In *Advances in Neural Information Processing Systems (NeurIPS)*, 2018. 2
- [100] Bolei Zhou, Agata Lapedriza, Aditya Khosla, Aude Oliva, and Antonio Torralba. Places: A 10 Million Image Database for Scene Recognition. In *IEEE Transactions on Pattern Analysis and Machine Intelligence (TPAMI)*, 2018. 6, 14
- [101] Kaiyang Zhou, Yongxin Yang, Timothy Hospedales, and Tao Xiang. Learning to Generate Novel Domains for Domain Generalization. In *Proceedings of the European Conference on Computer Vision (ECCV)*, 2020. 2
- [102] Kaiyang Zhou, Yongxin Yang, Yu Qiao, and Tao Xiang. Domain Generalization with MixStyle. In *International Conference on Learning Representations (ICLR)*, 2021. 2

# Robust 3D Shape Reconstruction in Zero-Shot from a Single Image in the Wild

## — Supplementary Material —

In this supplementary material, we provide more implementation details (Sec. A), training and evaluation details (Sec. B), analyses (Sec. C), discussion (Sec. D), and broader impacts with ethics considerations (Sec. E), which are not included in the main paper due to its space constraints.

### A. Implementation Details

#### A.1. Model Architecture

**Pixel-level regression.** We employ the backbone of DPT-Hybrid [68], which is composed of 12 transformer layers and 4 fusion layers. From the global feature map  $\mathbf{X}_G$ , we estimate parameters for camera intrinsics  $K$  using 4 convolutional layers, 2 ReLU activation layers, an average pooling layer, and a linear layer. From the fine-grained feature map  $\mathbf{X}_F$ , we regress the depth map  $\mathbf{M}_D$ , visible mask  $\mathbf{M}_V$ , and occluder mask  $\mathbf{M}_O$ . Specifically, the depth map  $\mathbf{M}_D$  is regressed using 3 convolutional layers, 2 ReLU activation layers, and a bilinear interpolation layer. The visible mask  $\mathbf{M}_V$  and occluder mask  $\mathbf{M}_O$  are regressed through 2 convolutional layers, 1 ReLU activation layer, and a bilinear interpolation layer, respectively. The scaling factor  $\gamma$  and shift factor  $\beta$  used for the affine transformation are estimated via a linear layer and a SiLU activation layer.

**3D point-wise regression.** From the concatenated output of the visible 3D shape  $\mathbf{S}_V$  and occluder mask  $\mathbf{M}_O$ , we extract features using the backbone of ResNet50 [30], augmented with additional 9 convolutional layers and 4 ReLU activation layers. These extracted features serve as keys and values in 2 cross-attention layers, where sine-cosine positional embeddings are incorporated to preserve spatial information. The cross-attention layers process queries constructed by the concatenation of point embeddings and text embeddings. The point embeddings are derived from 3D query points using 2 linear layers, while the text embeddings are obtained from CLIP text embeddings [67] projected by a linear layer. The outputs from the cross-attention layers are used to regress occupancy values of the 3D query points through 9 linear layers with skip connections and 8 Softplus activation layers.

#### A.2. Data Synthesis

The pseudocode for our data synthesis pipeline is outlined in Algorithm 1.

**Rendering.** We utilize the 3D shape renderings provided by ZeroShape [35]. These renderings were produced using Blender [9] with various camera configurations. Specifically, focal lengths were varied between 30mm and 70mm for a 35mm sensor size equivalent. Camera distances and

LookAt points were also randomized, with elevation angles ranging from  $5^\circ$  to  $65^\circ$ . These renderings, produced at a resolution of  $600 \times 600$  pixels, were cropped around the center of objects and resized to  $224 \times 224$  pixels.

**Object appearance diversification.** We utilize ControlNet [97] to simulate diverse visual variations in object appearances, excluding those with high-resolution texture maps (e.g., several objects from Objaverse [13]). To be specific, variations are generated by a textual condition “a [color] [material] [object]”, where [color] and [material] are randomly selected from pre-defined color list  $\mathcal{L}_c$  and material list  $\mathcal{L}_m$ , respectively. The color list  $\mathcal{L}_c$  includes “red”, “pink”, “orange”, “yellow”, “green”, “blue”, “purple”, “brown”, “white”, “black”, “gray”, and an empty string. The material list  $\mathcal{L}_m$  contains “metal”, “wood”, “plastic”, “ceramic”, “stone”, “rubber”, “leather”, and an empty string. To utilize more plausible and diverse textual conditions according to each object rendering, one can leverage suggestions from LMMs [45].

**Initial guidance.** As described in Section 4.2 of the main paper, we leveraged initial guidance to reduce silhouette distortion of objects. To be specific, when we utilized ControlNet [97], we set 20 steps in the DDIM sampler [75] and injected the guidance at step 8. This guidance effectively forces the conditional diffusion model to precisely adhere to input spatial condition.

**Filtering synthesized object images.** While the initial guidance substantially aids in preserving the object silhouette as specified in the spatial condition, minor disparities may still exist between the silhouettes in the synthesized images and the original silhouettes from the renderings. To address this, we filter out images if the intersection-over-union (IoU) between the synthesized and original silhouettes is below 0.95. The silhouettes in the synthesized images are estimated by extracting the foreground objects in the images. We can simply extract the foreground objects using a threshold, as the initial guidance results in images that have nearly-white backgrounds. Specifically, we convert each synthesized RGB image to grayscale, and then consider pixels with values between 250 and 255 as background. This straightforward process allows us to accurately approximate the foreground silhouette in most cases.

**Background diversification.** We simulate diverse backgrounds using an object-aware background outpainting model [16] with a textual condition “a [object] in the [scene]”, where [scene] is randomly selected from pre-defined scene list  $\mathcal{L}_s$ . As described in Section 4.3 of the main paper, we use scene categories from [90, 100] as the

---

**Algorithm 1** Pseudocode of our data synthesis pipeline

---

**Requirement:** object renderer  $\mathcal{R}(\cdot)$ , guidance perturbator  $\mathcal{P}(\cdot)$ , random seed generator  $\mathcal{G}(\cdot)$ , diffusion model for object diversification  $\text{DM}_{\text{obj}}(\cdot)$ , diffusion model for background outpainting  $\text{DM}_{\text{bg}}(\cdot)$

**Input:** 3D objects  $\{\mathcal{O}_i\}_{i=1}^K$ , number of camera views for rendering 3D objects  $\{N_i\}_{i=1}^K$ , color list  $\mathcal{L}_c$ , material list  $\mathcal{L}_m$ , scene list  $\mathcal{L}_s$ , IoU filtering threshold  $\kappa$

**Output:** (3D object, camera parameters, depth map, mask, image)–dataset

#  $\mathcal{C}$ : camera parameters,  $\mathcal{D}$ : depth map,  $\mathcal{M}$ : mask,  $\mathcal{I}$ : image

```
1:  $\{\mathcal{C}_{i,j}\}_{i=1,j=1}^{K,N_i}, \{\mathcal{D}_{i,j}\}_{i=1,j=1}^{K,N_i}, \{\mathcal{M}_{i,j}\}_{i=1,j=1}^{K,N_i}, \{\mathcal{I}_{i,j}\}_{i=1,j=1}^{K,N_i} \leftarrow \mathcal{R}(\{\mathcal{O}_i\}_{i=1}^K, \{N_i\}_{i=1}^K)$  ▷ render 3D objects
2: dataset  $\leftarrow []$ 
3: for  $i = 1, 2, \dots, K$  do
4:   for  $j = 1, 2, \dots, N_i$  do
5:     guide  $\leftarrow \mathcal{P}(\mathcal{I}_{i,j})$  ▷ perturb an initial guidance
6:     while True do
7:       seed  $\leftarrow \mathcal{G}()$  ▷ set random seed
8:       [color], [material]  $\leftarrow \text{sample}(\mathcal{L}_c, \mathcal{L}_m, \text{seed})$  ▷ randomly select words
9:       [object]  $\leftarrow \text{retrieve\_category}(\mathcal{O}_i)$  ▷ retrieve 3D object category
10:      txt  $\leftarrow$  "a [color] [material] [object]"
11:      fg_img  $\leftarrow \text{DM}_{\text{obj}}(\mathcal{D}_{i,j}, \text{guide}, \text{txt}, \text{seed})$  ▷ simulate object appearance
12:      if not is_filtered(fg_img,  $\mathcal{M}_{i,j}, \kappa$ ) then ▷ filter an image with a threshold  $\kappa$ 
13:        | break
14:      end if
15:    end while
16:    seed  $\leftarrow \mathcal{G}()$  ▷ set random seed
17:    [scene]  $\leftarrow \text{sample}(\mathcal{L}_s, \text{seed})$  ▷ randomly select a word
18:    txt  $\leftarrow$  "a [object] in the [scene]"
19:    fg_bg_img  $\leftarrow \text{DM}_{\text{bg}}(\mathcal{M}_{i,j}, \text{fg\_img}, \text{txt}, \text{seed})$  ▷ simulate background
20:    Add  $(\mathcal{O}_i, \mathcal{C}_{i,j}, \mathcal{D}_{i,j}, \mathcal{M}_{i,j}, \text{fg\_bg\_img})$  to dataset
21:   end for
22: end for
23: return dataset
```

---

scene list  $\mathcal{L}_s$ , which contains more than 700 categories. To utilize more plausible and diverse textual conditions according to each foreground object, one can leverage suggestions from LMMs [45].

## B. Training and Evaluation Details

We initialize our model with ZeroShape [35] model weights for shared components such as DPT-Hybrid backbone [68] and cross-attention layers. We first pre-train our pixel-level regression components for 10 epochs, using the Adam optimizer [38] with a learning rate of  $10^{-5}$ , a batch size of 80, a weight decay of 0.05, and momentum parameters of (0.9, 0.95). This process takes approximately 2 days on 4 RTX 3090 GPUs. Then, we train our entire model for 15 epochs, using the same optimizer with a learning rate of  $10^{-5}$  for 3D point-wise regression components and  $10^{-6}$  for pre-trained pixel-level regression components, a batch size of 80, a weight decay of 0.05 and momentum parameters of (0.9, 0.95). This process takes approximately 4 days on 4 RTX 3090 GPUs.

**Loss coefficients.** Let  $\mathcal{L}_c$  represent the camera intrinsics loss,  $\mathcal{L}_d$  the depth loss using ground-truth depth values,  $\mathcal{L}_d^{\text{aux}}$  the auxiliary depth loss using depth values estimated from Depth Anything V2 [93],  $\mathcal{L}_m^{\text{vis}}$  the visible mask loss,  $\mathcal{L}_m^{\text{occ}}$  the occluder mask loss, and  $\mathcal{L}_o$  the occupancy loss. The loss  $\mathcal{L}$  used for training the pixel-level regression components is computed as follows:

$$\mathcal{L} = \lambda_c \mathcal{L}_c + \lambda_d \mathcal{L}_d + \lambda_d^{\text{aux}} \mathcal{L}_d^{\text{aux}} + \lambda_m^{\text{vis}} \mathcal{L}_m^{\text{vis}} + \lambda_m^{\text{occ}} \mathcal{L}_m^{\text{occ}}, \quad (3)$$

where  $\lambda_c = 10$ ,  $\lambda_d = \lambda_m^{\text{vis}} = \lambda_m^{\text{occ}} = 1$ , and  $\lambda_d^{\text{aux}} = 0.1$ . The loss  $\mathcal{L}'$  used for training our entire model is computed as follows:

$$\mathcal{L}' = \mathcal{L} + \lambda_o \mathcal{L}_o, \quad (4)$$

where  $\lambda_o = 1$ . To compute the occupancy loss  $\mathcal{L}_o$ , we randomly sample 4096 query points at every iteration.

**Copy-Paste augmentation.** As shown in Figure B1, we apply the augmentation by randomly selecting objects synthesized with focal lengths similar to the corresponding training sample. In each training iteration, we randomly choose from 0 to 2 occluders, resize them within a scale range of 0.4 to 0.6, and put them onto the training sample.



Figure B1. Examples of Copy-Paste augmentation. In this visualization, we provide augmented training samples with occluder masks.

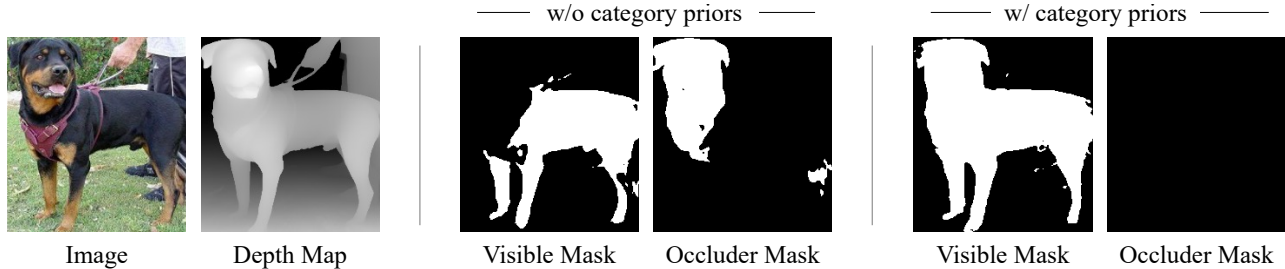


Figure C1. Effect of category priors on mask regression. Without utilizing the priors, the regression of visible and occluder masks appears to rely on depth values. By leveraging the priors, the regression is enhanced with semantic understanding.

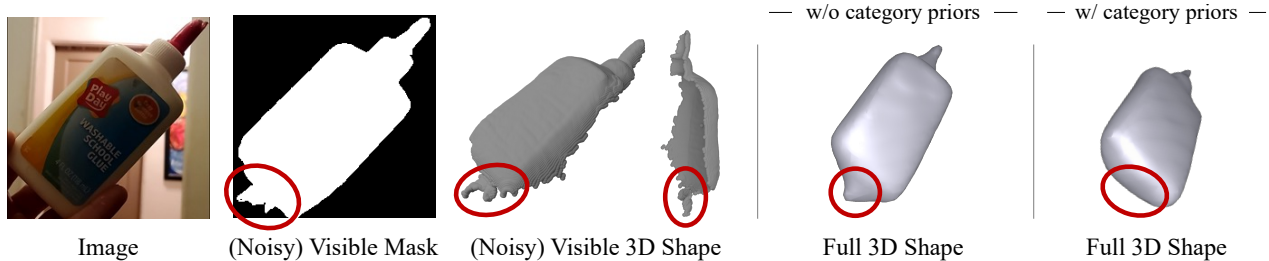


Figure C2. Effect of category priors on occupancy regression. Without utilizing the priors, it is challenging to distinguish the object from its background in the noisy visible 3D shape. By leveraging the priors, the regression is enhanced with learned 3D shape prior specific to the category, leading to more accurate results. We highlight regions with red circles.

**Category priors.** We use CLIP text embeddings [67] to learn category-specific priors with ground-truth object categories from Objaverse-LVIS [13] and ShapeNetCore.v2 [5].

**Evaluation.** For the quantitative evaluation of our model, we compute Chamfer Distance (CD) and F-Score (FS). Regarding  $FS@\tau$ , we set the distance threshold  $\tau$  to 0.05. For the evaluation, we need to convert implicit 3D shapes into explicit meshes and then sample points from their surfaces. To obtain explicit meshes, we apply Marching Cubes [50] algorithm, using sampled values from a  $128^3$  spatial grid.

**Estimation of object category.** To incorporate category-specific priors, we optionally estimate the object category of an object-centric image using a VLM [45]. We use the following prompt: *What is the salient object in this image? The object should occupy the majority of the image. Please provide the category name of the salient object in the format: “[object]”, where “[object]” is the specific category name (e.g., “chair”, “bed”, “sofa”, “table”).*

## C. More Analyses

**Category priors for regressing masks.** When category priors are not utilized, our model sometimes incorrectly splits a single entity (e.g., a dog) into visible region (e.g., the dog’s body) and occluder region (e.g., the dog’s head) based on depth values, as shown in Figure C1. We suspect this issue arises due to the lack of semantic understanding. To mitigate this, one may incorporate semantic priors by estimating object categories using a vision-language model.

**Category priors for regressing occupancy values.** Visible 3D shapes may include background geometries due to noisy estimations of visible masks. In such cases, it is challenging to accurately regress occupancy values for the corresponding objects. To be specific, distinguishing a salient object from its background is difficult, because a visible 3D shape only contains the xyz-coordinates of each pixel (i.e., pixel-aligned point cloud) without any supplemental visual cues (e.g., RGB color). To address this issue, one may leverage category priors for regressing the occupancy values, as shown in Figure C2.



Figure D1. Observations from pre-trained conditional generative models [44, 57, 66, 97]. This phenomenon is mainly attributed to their pre-training procedure; they were trained with depth maps which contain both foreground and background information. When we use depth maps rendered from 3D objects, synthesizing backgrounds violates input spatial conditions.

## D. Discussion

**Why synthesizing images in two steps?** Our data synthesis pipeline first generates foreground objects and then outpaints their backgrounds. A more straightforward alternative would be to synthesize the entire image at once using conditional generative models such as ControlNet [97]. However, as shown in Figure D1, when these models are forced to strictly follow the input spatial conditions, they often produce monotonous backgrounds due to the lack of background information in the conditions. On the other hand, if we encourage the models to diversify backgrounds using textual conditions, they tend to create more varied backgrounds at the cost of violating the input spatial conditions. To resolve these challenges, we first diversify object appearances while adhering to the input spatial conditions, and then use an object-aware background outpainting model [16], specifically fine-tuned to prevent distortion of object silhouettes while generating the backgrounds.

**Various approaches for occlusion-aware reconstruction.** Probabilistic methods (*e.g.*, PT43D [91]) are effective for handling heavily occluded objects by generating multiple plausible 3D shapes. However, there are trade-offs between (i) accuracy and sample diversity [72], and (ii) accuracy and efficiency [22]. In comparison, regression-based methods can efficiently produce competitive results for small occlusions, but they become sub-optimal and often impractical when tackling highly occluded objects.

## E. Broader Impacts & Ethics Considerations

Our data synthesis pipeline utilizes 3D object collections and conditional generative models. To avoid conflicts, one should carefully follow their usage rights, licenses and permissions. Also, one should be aware that generative models might reflect biases inherent in their training data [17], and object images in the training data might also be biased [10]. Furthermore, one should keep in mind that generative mod-

els might expose their training data [3]. To avoid data privacy issues, one can use erasing methods [21, 58] capable of removing unwanted concepts from generative models.